PCCP

PAPER

View Article Online
View Journal | View Issue

Cite this: *Phys. Chem. Chem. Phys.*, 2016, **18**, 28198

Aggregates of quadrupolar dyes for two-photon absorption: the role of intermolecular interactions†

S. Sanyal,[a] A. Painelli,[a] S. K. Pati,[b] F. Terenziani[a] and C. Sissa*[a]

Received 25th July 2016,
Accepted 11th September 2016

DOI: 10.1039/c6cp05153g

www.rsc.org/pccp

We present a theoretical investigation of small aggregates of quadrupolar (A–π–D–π–A or D–π–A–π–D) charge-transfer dyes, with attention focused on the role of intermolecular interactions in determining their optical properties. We tackle the theoretical issue by adopting essential-state models (ESMs), which describe an isolated molecule in terms of a minimal number of electronic states, corresponding to the resonance structures. ESMs quite naturally describe intermolecular interactions relaxing the dipolar approximation and accounting for molecular polarizabilities. The approach is applied to curcuminoid and squaraine dyes, two families of chromophores with weak and strong quadrupolar character, respectively. The method is validated against experiment and for curcuminoids also against time-dependent density functional theory. ESMs rationalize the strong ultra-excitonic effects recurrently observed in the experimental optical spectra of aggregates of highly polarizable quadrupolar dyes, offering a valuable tool to exploit the supramolecular design of material properties.

Introduction

Intermolecular electrostatic interactions are the driving force of two key phenomena in molecular functional materials: energy transfer and energy delocalization. Energy transfer is an incoherent process where an excited molecule, the energy donor, transfers its excess energy to a nearby energy acceptor.[1–3] Being driven by long-range electrostatic interactions, energy transfer occurs up to comparatively large distances (~100 Å) and requires the resonance between the de-excitation energy of the donor (from its relaxed excited state) and the absorption energy of the acceptor. Energy delocalization instead occurs when electrostatic interactions are larger than the difference between the transition energies of nearby molecules, giving rise to Frenkel excitons.[4,5] Energy delocalization governs the spectral properties of molecular crystals and aggregates, where intermolecular distances can be comparable to or even smaller than the sum of van der Waals radii. The simplest models for either phenomenon rely on the dipolar approximation for intermolecular interactions, directly relating the two processes and their measurable effects to experimentally accessible data for the isolated molecules, and specifically to the transition dipole moments of the relevant excitations. As originally derived by Förster,[6,7] the rate of energy transfer (often called Förster resonance energy transfer, FRET) goes with the product of the squared transition dipole moments for the emission of the energy donor and the absorption of the energy acceptor, while the exciton splitting in a dimeric structure (or the exciton band-width in a molecular crystal) is proportional to the inner product of the transition dipole moments of nearby molecules.[4,5] Therefore, in the dipolar approximation, only optically allowed states (*i.e.* states having a sizable transition dipole moment from the ground state) are of relevance either for energy-transfer processes or for exciton delocalization. However, the dipolar approximation fails whenever intermolecular distances are comparable to or smaller than the molecular dimensions: the involvement of dark (optically forbidden) states in energy transfer processes has been extensively discussed in the literature,[8–12] and several suggestions have been given about the exciton coupling of dark states.[13,14] A second, somewhat subtler approximation usually enters the standard models for either energy transfer or energy delocalization, and amounts to neglecting the molecular polarizability. In other terms, it is assumed that the charge distribution on each molecule, in the ground or excited state, is not affected by the presence of nearby molecules, a fairly poor approximation for largely polarizable molecules in molecular aggregates and crystals where intermolecular distances are small.[15,16]

In this context, charge-transfer (CT) dyes, a large family of π-conjugated molecules where the presence of electron donor (D)

[a] *Dipartimento di Chimica, Parco Area delle Scienze 17/A, 43124 Parma, Italy. E-mail: cristina.sissa@unipr.it*
[b] *Theoretical Sciences Unit and New Chemistry Unit, JNCASR, Jakkur P. O., Bangalore 560064, India*

† Electronic supplementary information (ESI) available. See DOI: 10.1039/c6cp05153g

and/or acceptor (A) groups leads to low-energy excitations with large polarizabilities, are particularly interesting. The low-energy physics and the linear and nonlinear optical properties of CT dyes are well captured by essential-state models (ESMs),[17–24] a family of parametric Hamiltonians that describe the electronic structure of CT dyes in terms of a few diabatic basis states, corresponding to the main resonating structures. The coupling to molecular vibrations and polar solvation leads to a quite accurate description of the complex spectral behavior of these molecules in different environments. ESMs also naturally describe the intermolecular interactions relaxing the dipolar approximation and fully accounting for the molecular polarizability.[14–16,25] The applicability of ESMs to energy-transfer processes has been validated by a direct comparison with time dependent density functional theory (TDDFT) calculations.[12,26] The reliability of ESMs to describe the effects of intermolecular interactions in linear and nonlinear optical spectra of a few model systems has been validated experimentally.[14,27–34] For aggregates or crystals of polar (D–π–A) dyes, ESMs predict strong ultra-excitonic effects,[16] eventually leading to multiexciton generation[15] and phase coexistence,[35–37] while biexciton states in aggregates of quadrupolar (D–π–A–π–D or A–π–D–π–A) dyes have been suggested as a way towards amplified two-photon absorption (2PA).[14]

In this paper, we apply ESMs to aggregates of quadrupolar dyes, validating the results against quantum chemical calculations. The models are subsequently exploited as a reliable and flexible tool to understand the spectral properties of organic nanoparticles based on quadrupolar dyes. Indeed, quadrupolar dyes are actively investigated as structures of choice for 2PA applications in bio-imaging, nanofabrication, photodynamic therapy, *etc.* Typical 2PA dyes include squaraines,[38–45] fluorene-based chromophores,[46–51] and distrylbenzenes,[52–54] to name a few. These dyes, designed for large 2PA cross-sections, are in general poorly soluble in water and biological media. Different strategies (including encapsulation in micelles,[55] dispersion in silica nanoparticles,[56] preparation of supramolecular assemblies[57]) are exploited to make hydrophobic dyes suitable for biological applications. Among different methods, organic nanoparticles (ONPs) offer a simple and versatile approach to disperse nano-sized agglomerates of dyes in water.[57–61] For application purposes, it is important that ONPs are stable and maintain or possibly improve the optical properties of the dye. Specifically, for 2-photon imaging applications, the active species must have a large 2PA cross-section and a large fluorescence quantum yield, a delicate issue for ONPs in view of the self-quenching of fluorescence often observed in condensed phases. Nevertheless, several interesting examples of fluorescent organic nanoparticles (FONs) are known with large fluorescence quantum yields,[58,60,62] and sometimes amplified 2PA response.[59] However, most ONPs based on quadrupolar dyes show a strongly reduced fluorescence.[63–65] In this work we will set the basis to understand this phenomenon, offering suggestions for the optimized design of aggregates of quadrupolar dyes. We will focus the attention on two different families of chromophores: boron-difluoride-curcuminoids (hereafter curcumins, see **1** in Fig. 1) and squaraines (see **2** and **3** in Fig. 1). Curcumins offer the possibility to validate the essential-state approach not only against the experiment, but also against TDDFT calculations. Squaraines were selected as interesting systems showing unusual aggregation effects[40,41,66] even if the well-known problems of TDDFT in dealing with squaraines,[67–69] hinders a thorough computational analysis of these systems.

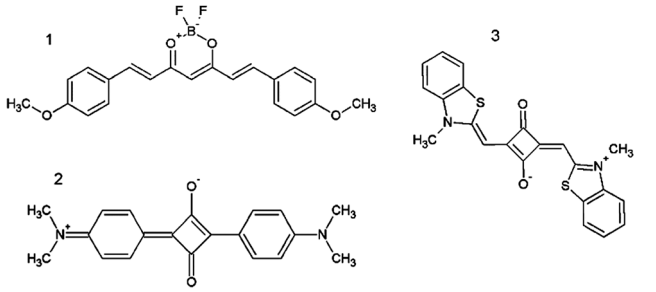

Fig. 1 Structures of the investigated molecules.

Theoretical methods

TDDFT calculations

Ground-state geometry optimizations were performed using density functional theory (DFT), as implemented in the GAUSSIAN09[70] software package using the 6-31+g(d) basis set for all atoms. We confirmed the stability of the obtained geometries by ruling out the presence of imaginary frequencies. The ground-state geometry of the isolated molecule **1** in the gas phase was optimized employing the B3LYP (Becke, three-parameter, Lee–Yang–Parr)[71] hybrid exchange and correlation energy functional, while the long-range dispersion corrected non-local energy functional, ωB97XD,[72] was employed for the geometry optimization of dimers to account for dispersion corrections. Solvation effects in dichloromethane (DCM) were included adopting the polarizable continuum model (PCM).[73]

TDDFT calculations were performed using the long-range corrected (LRC) version of B3LYP, the Coulomb-attenuating method (CAM-B3LYP)[74] and the 6-31+g(d) basis set. We used the LRC density functional to properly describe CT states. TDDFT calculations were run for **1** in the gas phase and DCM solvent. We studied two different molecular dimers, whose geometries were extracted from the crystal structure. The evolution with the intermolecular distance of the spectral properties of both dimers was investigated.

The transition intensity for the linear (one photon) absorption (1PA) is expressed in terms of oscillator strength defined as (atomic units):

$$f = \frac{2\omega_n}{3}|\langle 0|\mu|n\rangle|^2$$

where ω_n is the excitation frequency of the $|n\rangle$ state and μ is the electric dipole moment operator.

The DALTON2015 package[75] was used to calculate the two-photon absorption (2PA) spectra of **1** in the gas phase and solution and those of molecular dimers in the gas phase, using the CAM-B3LYP functional and the 6-31+g(d) basis set. The 2PA intensity

(δ_{2PA}) is calculated, for a linearly polarized monochromatic beam of light, as follows:[76–78]

$$\delta_{2PA}(\omega) = \sum_{kl} 2S_{kk}(\omega)S_{ll}(\omega) + 4S_{kl}(\omega)S_{kl}(\omega)$$

where $S(\omega)$ is the 2PA tensor.[75] The 2PA cross-section is finally obtained (assuming a Lorentzian bandshape) as:

$$\sigma_{2PA}(\omega) = \frac{4\pi^3\alpha a_0^5}{15c}\frac{\omega^2}{\Gamma}\delta_{2PA}(\omega)$$

where a_0, c and α are the Bohr radius, the speed of light and the fine structure constant, respectively, while Γ (set to 0.1 eV) is the full width at half maximum of the Lorentzian lineshape.

ESM for quadrupolar dyes and their aggregates

The 3-state model for quadrupolar dyes,[19] proposed in 2006, has been validated against experimental data for several families of dyes, including fluorene-based dyes, squaraines, substituted distyrylbenzenes, cyanines, *etc.*[27,79–82] More recently, the 3-state model has been extended to account for a fourth state, as relevant for cyanine dyes.[83] The 3-state model for an isolated D–π–A–π–D (or equivalently A–π–D–π–A) quadrupolar dye considers three diabatic basis states, corresponding to three main resonating structures: the neutral state N, and two degenerate zwitterionic states, Z_1 and Z_2, as sketched in panel a of Fig. 2. Only two parameters enter the electronic model: 2η, the energy gap between the two degenerate zwitterionic states and the neutral state, and τ, the mixing element between N and Z_1 and Z_2. The dipole moment operator has only two non-vanishing terms, corresponding to the permanent dipole moments of Z_1 and Z_2, which are aligned along the molecular axis and have opposite directions for the two states. The model parameter μ_0 represents the magnitude of the permanent dipole moments of Z_1 and Z_2, and is required to calculate the intensity of optical spectra.

A symmetrized basis set is conveniently introduced: N and $Z_\pm = (Z_1 \pm Z_2)/\sqrt{2}$. On this basis, the ground state, g, is a linear combination of N and Z_+, where the weight of Z_+ measures the quadrupolar character of the dye, *i.e.* the charge residing on the central group: $\rho = 0.5\left(1 - \eta\Big/\sqrt{\eta^2 + 2\tau^2}\right)$. Two excited states are obtained with opposite parity: a bright ungerade state c, corresponding to Z_- (which remains unmixed), and the dark gerade state e, the N and Z_+ combination orthogonal to g.

This simple three-state electronic model captures the essential features of quadrupolar dyes, with the bright state located at a lower energy than the dark, 2PA-active state. In more detail, dyes with low ρ values ($2\eta/\tau \gg 1$) have almost degenerate 1PA-active (c) and 2PA-active (e) states, driving the system towards excited-state symmetry breaking (class I dyes).[19] Dyes with high ρ values ($2\eta/\tau \ll -1$) have a small energy gap between the ground and the

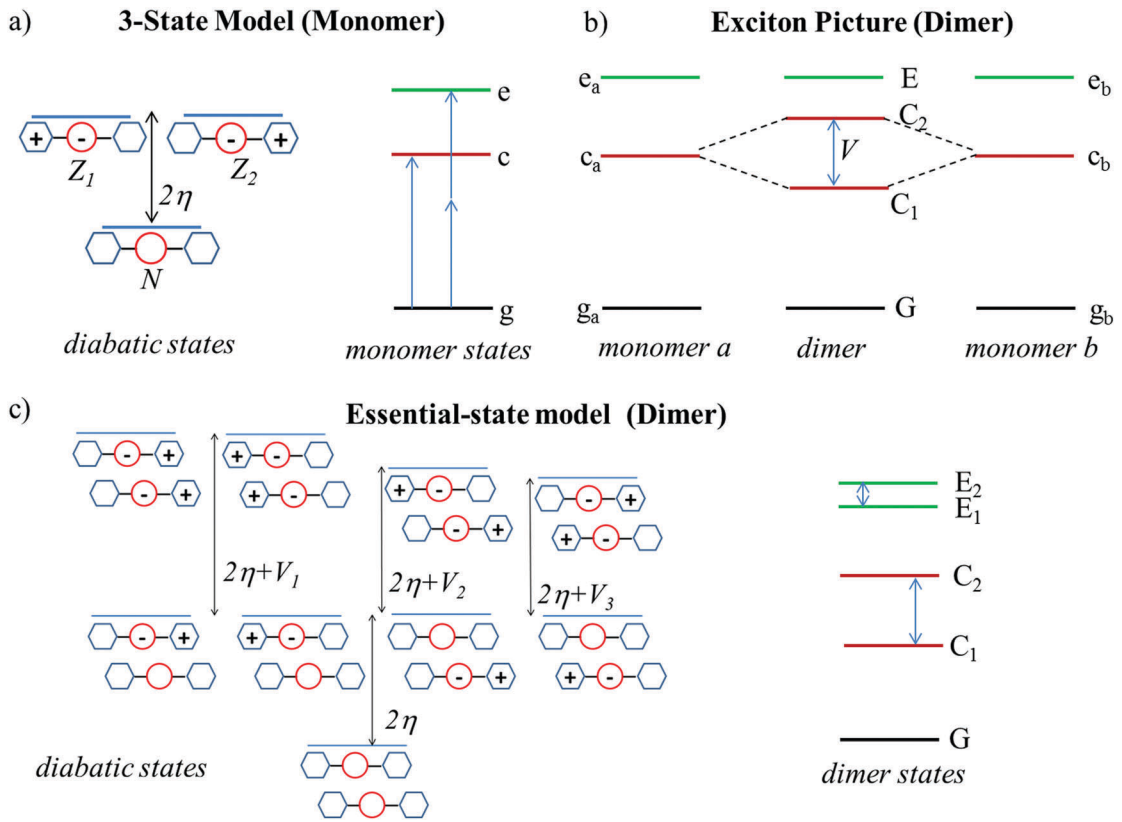

Fig. 2 Panel a: sketch of the 3-state model for quadrupolar dyes. Panel b: the exciton picture of a dimer. Panel c: ESM of a dimer. Complete expressions for electrostatic interactions are reported in the ESI† (Fig. S1 and S2).

1PA-active states, leading the system towards ground-state instability (class III dyes).[79] Systems with intermediate ρ ($2\eta \cong \tau$) have the 1PA-active state lying almost midway between the ground state and the 2PA-active state, with amplified 2PA and no tendency to symmetry breaking (class II).[19]

The exciton model is the prevailing approach to intermolecular interactions in molecular aggregates or crystals and, as sketched in Fig. 2b, corresponds to a zeroth-order perturbative treatment of intermolecular interactions. Accordingly, only degenerate states are mixed by the interaction, leading to the splitting of the two singly-excited states in a dimer and to the formation of the single-exciton band in molecular crystals or large aggregates. The exciton model fully neglects the molecular polarizability and does not account for any charge redistribution in the molecule as a result of the interactions. This is a particularly poor approximation for largely polarizable molecules. The dipolar approximation for intermolecular interactions is a further common approximation adopted in the exciton model. As sketched in Fig. 2b for dimers of quadrupolar dyes, in the dipolar approximation, the 2PA-active states are not affected by aggregation phenomena.

ESMs easily overcome both approximations. Specifically, as shown in Fig. 2c for a molecular dimer, diabatic basis states are constructed for the aggregate as the direct product of the monomers' states. On this basis, the Hamiltonian for the aggregate is easily obtained from the molecular Hamiltonian, with electrostatic intermolecular interactions affecting the energy of basis states where two or more molecules are in a zwitterionic state. The diagonalization of the diabatic Hamiltonian yields adiabatic states fully accounting for electrostatic intermolecular interactions as well as for the molecular polarizability (see Fig. 2c).

Different approaches can be adopted to estimate electrostatic interactions among diabatic states. Here the electrostatic interactions are described in terms of interaction among integer point-charges at the D and A sites of the zwitterionic basis states (see Fig. S1 and S2 of the ESI† for explicit expressions). The resulting extended-dipole approximation represents a simple but effective way to describe interactions between molecules whose dimensions are comparable to the intermolecular distance.[9,11,12,15,25,26]

We stress here that electrostatic intermolecular interactions entering the ESMs are relevant to the diabatic states, *i.e.* the basis states. These states, corresponding to the main molecular resonating structures, are characterized by integer charges. However, the states relevant to spectroscopy are the adiabatic eigenstates, typically characterized by fractional charges. For example, the ground state charge distribution for each dye is defined as $D^{+\rho/2}A^{-\rho}D^{+\rho/2}$ with ρ values comprised between 0 and 1 ($\rho \sim 0.2$ for curcumin dyes and $\rho \sim 0.3$–0.5 for squaraine dyes).

The number of diabatic basis states for aggregates of quadrupolar dyes increases as 3^N, where N is the number of molecules, so that fairly large aggregates can be easily described, particularly in view of the sparse nature of the Hamiltonian matrix. In the following, we will describe the optical spectra calculated for aggregates of different sizes, imposing open boundary conditions and only accounting for the nearest-neighbor interactions. One-photon absorption and fluorescence spectra are calculated assigning Gaussian lineshapes to allowed transitions with full-width at half maximum Γ. Two-photon absorption spectra are calculated using the SOS expression,[84,85] where the sum runs over all electronic excited states.

Validating ESM *via* TD-DFT calculations: the case of curcumin dyes

Modeling the isolated molecules

A recent paper[63] reports on the spectral properties of nanoparticles of boron-difluoride-curcuminoids (hereafter curcumins). Curcumins show a marginal absorption solvatochromism and a well-pronounced emission solvatochromism.[86,87] Accordingly, they can be safely classified as class I quadrupolar dyes,[19] the weak absorption solvatochromism being due to the V-shape of molecular geometry.[80,88] With reference to dye **1** in Fig. 1, two transitions are observed in the visible range: the lowest-energy transition (at 2.54 eV in dichloromethane, DCM), corresponding to state c, is strongly allowed in 1PA, and has weak 2PA intensity, while the second transition, at 3.22 eV in DCM, assigned to the e-state, is strongly 2PA-allowed and has weak 1PA intensity. The proximity of the c and e states is another signature of class I dyes.

In curcumin-based ONPs, 1PA spectra are blue-shifted (and broadened) compared to solution spectra, while in emission spectra a sizeable red-shift and a marked decrease of intensity is observed (similar effects are also observed in the emission spectra of crystals). The spectral position of the 2PA band is marginally affected by aggregation, with (weak) enhancement of intensity in ONPs. The exciton picture qualitatively rationalizes the spectral behavior of aggregates of curcumin dyes: the blue-shift of the absorption band and the strong decrease of fluorescence intensity are consistent with H-type aggregation, as observed for crystals.[63] Moreover, the exciton picture supports marginal aggregation effects on 2PA.

Table 1 Experimental data from ref. 63 and TDDFT results for curcumin **1**

	Experimental data in ref. 63			Calculated (gas phase)			
	Transition wavelength (energy)	Molar extinction coefficient (M^{-1} cm^{-1})	σ_{2PA}[a] (GM)	Transition wavelength (energy)	Oscillator strength	Nature of transitions	σ_{2PA}[a] (GM)
g → c	488 nm (2.54 eV)	75 480	<10	378 nm (3.28 eV)	2.11	h → l (90%)	17
g → e	385 nm (3.22 eV)	~10 000	155	304 nm (4.08 eV)	0.08	h−1 → l (90%)	2030

[a] GM = Göpper-Mayer. 1 GM = 10^{-50} cm^4 s $photon^{-1}$.

Table 1 compares experimental data for dye **1** in solution with TDDFT results (gas phase, crystallographic geometry, and planar molecule; additional results can be found in the ESI,† Fig. S3–S5 and Tables S1 and S2). In agreement with experimental results, the lowest transition (g → c) has a large oscillator strength, but a very weak 2PA cross-section, while the second transition (g → e) is marginally allowed in 1PA and has strong 2PA activity (we notice that the Dalton estimate of σ_{2PA} assumes a linewidth Γ = 0.1 eV. To account for the broader experimenatal linewidth, the estimated σ value should be reduced by a factor of 3). When compared with experiment, TDDFT transition energies are overestimated by ∼0.8 eV. As expected, TDDFT results obtained for solvated molecules (see ESI,† Table S2) reduce the discrepancy. Further improvement could be obtained accounting for molecular vibrations.[89] Our results are in agreement with a recent work about experimental and theoretical investigations of a family of curcumin dyes.[87]

The g → c and g → e transitions, largely dominated by the h → l and h → l−1 configurations (h = monomer HOMO, l = monomer LUMO), have a clear intramolecular charge-transfer character, as shown by the frontier molecular orbitals in Fig. 3a, and can be readily identified with the g → c and g → e transitions of the ESM.

The experimental 1PA and 2PA energies fix the two parameters entering the electronic ESM Hamiltonian for **1** as η = 0.94 eV and τ = 0.93 eV, corresponding to class I quadrupolar dyes, with $\rho \sim 0.2$. The experimental molar extinction coefficient is fixed at μ_0 = 20 D, which, in turn allows the estimation of $\sigma_{2PA} \sim 1100$ GM (Γ = 0.28 eV). Accounting for the screening effects (related to the squared refractive index) would reduce the ESMs estimated to be ∼ 500 GM, leading to a reasonable agreement with the experimental result.

Modelling curcumin aggregates

The crystal structure of **1** shows the presence of curcumin tetramers of the form T–P–P–T, where P and T represent two crystallographically inequivalent curcumin molecules, in a planar (P) and slightly twisted (T) geometry (see Fig. S3, ESI†). Since TDDFT calculations are not viable for tetrameric structures, in order to validate the ESM approach, we discuss the TDDFT results (at same level of theory as employed for the monomer) on dimers in crystallographic geometry, as well as in artificial geometries, where the intermolecular distance (r) is increased up to ∼9 Å in steps of 1 Å.

Tables 2 and 3 summarize the results of TDDFT calculations for the curcumin P–P dimer at the crystallographic distance (r = 3.74 Å) and at the artificially augmented distance of 6.74 Å. The results regarding other r values as well as for T–P dimers can be found in the ESI.† Fig. 3 shows relevant frontier orbitals together with their (approximate) relation to the frontier orbitals of the monomer (for the sake of clarity, we use lower-case letters, h and l, to refer to the molecular HOMO and LUMO, respectively, with indices a and b referring to each one of the two molecules in the dimer, when relevant; we use capital letters H and L for the HOMO and the LUMO of the dimer). As expected, each pair of equivalent molecular orbitals gives rise to two dimer orbitals

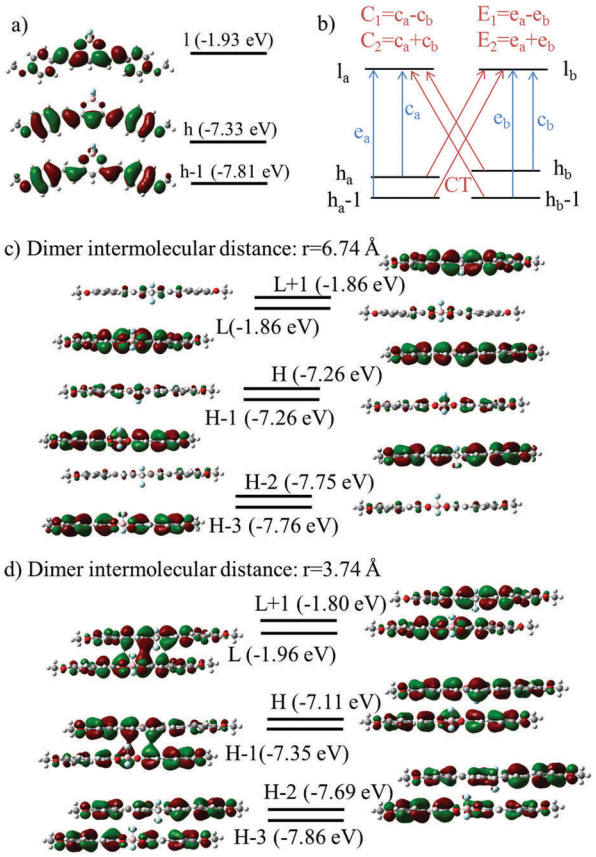

Fig. 3 (a) Frontier molecular orbitals of monomer of **1**; (b) sketch of the transitions expected for the dimer based on the monomer frontier orbitals; (c) frontier molecular orbitals for the dimer at r = 6.74 Å; and (d) frontier molecular orbitals of the dimer in crystallographic geometry (r = 3.74 Å).

Table 2 TDDFT results on the P–P dimer at r = 6.74 Å

Transition	Energy [eV]	Oscillator strength	δ_{2PA} [a.u.] (σ_{2PA} [GM])	Nature of the transition (>15%)
$S_0 \rightarrow S_1$ (C_1)	3.20	0.00	3883 (29)	H−1 → L (29%) c_a H → L+1 (28%) c_b H−1 → L+1 (16%) CT H → L (17%) CT
$S_0 \rightarrow S_2$ (C_2)	3.34	4.05	0.41 (—)	H−1 → L (44%) c_a H → L+1 (45%) c_b
$S_0 \rightarrow S_3$ (E_1)	4.04	0.15	48.80 (—)	H−3 → L (33%) e_a H−2 → L+1 (31%) e_b
$S_0 \rightarrow S_4$ (E_2)	4.11	0.00	2.5×10^5 (3090)	H−3 → L (44%) e_a H−2 → L+1 (46%) e_b
$S_0 \rightarrow S_5$	4.27	0.00	0.25 (—)	H → L (77%) CT
$S_0 \rightarrow S_6$	4.28	0.00	0.24 (—)	H−1 → L+1 (78%) CT

that are basically degenerate at large distances and weakly interact in crystallographic geometry (the calculated splitting amounts to ∼0.2 eV). As sketched in Fig. 3b, the h → l or c-transition of the monomer gives rise in the dimer to 4 transitions corresponding to the two c-transitions on each monomer (c_a and c_b in the figure) and two intermolecular charge-transfer transitions (CT in the figure). The two local transitions combine, in turn, in the C_1 and C_2 dimer exciton states. Similarly, the h−1 → l or e-transition of the monomers gives rise to the E_1 and E_2 dimer exciton states

Table 3 TDDFT results on the P–P dimer at r = 3.74 Å

Transition	Energy [eV]	Oscillator strength	δ_{2PA} [a.u.] (σ_{2PA} [GM])	Nature of the transition (>15%)
$S_0 \rightarrow S_1$ (C_1)	3.00	0.00	4907 (32)	H → L (72%) c_a–c_b, CT H−1 → L+1 (17%) c_a–c_b, CT
$S_0 \rightarrow S_2$ (C_2)	3.35	3.62	0.53 (—)	H → L+1 (66%) c_a + c_b, CT H−1 → L (18%) c_a + c_b, CT
$S_0 \rightarrow S_3$	3.60	0.34	4.69 (—)	H−1 → L (74%) c_a + c_b, CT H → L+1 (18%) c_a + c_b, CT
$S_0 \rightarrow S_4$	3.66	0.00	1459.4 (14)	H−1 → L+1 (73%) c_a–c_b, CT H → L (19%) c_a–c_b, CT
$S_0 \rightarrow S_5$ (E_1)	3.94	0.10	4.40 (—)	H−2 → L (57%) e_a–e_b, CT H−3 → L+1 (22%) e_a–e_b, CT
$S_0 \rightarrow S_6$ (E_2)	4.11	0.00	2.04×10^5 (2520)	H−2 → L+1 (52%) e_a + e_b, CT H−3 → L (36%) e_a + e_b, CT

and to intermolecular CT transitions. Along these lines, and based on the correspondence between the molecular and dimer orbitals (see Fig. 3c and d), we map the dimer transitions (or at least their main contributions) onto linear combinations of the molecular c_a, c_b, e_a and e_b transitions and of intermolecular CT transitions (see the last columns of Tables 2 and 3 and the corresponding results in the ESI†).

At large distances, the CT contribution to low-energy excitons is marginal and the first four dimer excited states can be safely mapped onto the four states, C_1, C_2, E_1, and E_2 defined in Tables 2 and 3. The energy of CT states decreases at short distances, making the excitation spectrum more crowded. We assign the two lowest states stemming from monomer c-excitations to C_1 and C_2, and the two lowest states stemming from monomer e-transitions to E_1 and E_2. A similar analysis is done for intermolecular distances varying from 3.74 Å to 7.74 Å (see ESI†) allowing us to estimate the energies for the four exciton states, as reported in Fig. 4.

In a bottom-up modeling approach, the ESM for the dimer is built starting from the electronic model for the monomer, defined by the two energies, η and τ estimated from the 1PA and 2PA frequencies, and introduces the intermolecular electrostatic interactions in the basis states, as discussed above. To such an aim, we need geometrical parameters. We set the length of the molecular arm to 6.5 Å and for the P–P dimer we fix the lateral shift d = 3.05 Å. The intermolecular distance r is varied from 3.74 up to 7.74 Å by steps of 1 Å. The diagonalization of the Hamiltonian matrix leads to the adiabatic eigenstates, as relevant to spectroscopy. As expected, based on simple physical considerations, only the first four excited states are relevant to low-energy spectroscopy (see Table 4 and ESI†): higher-energy states correspond to states where both molecules are excited. Looking in more detail, the first two excited states stem from the exciton splitting of the molecular c states. Specifically, the lowest-energy state C_1 is a dark state, and the spectral intensity of the two molecules is transferred to the second excited state, C_2, as expected for H-aggregates. The second pair of states, E_1 and E_2, stems out from the e molecular states. Their splitting is due to excitonic effects beyond the dipolar approximation. Both states are dark in 1PA, and the 2PA intensity from the molecular e-state is found on E_2, while E_1 is not seen in either 1PA or 2PA spectra. The C_2–C_1 and E_2–E_1 splittings both decrease with increasing r, with the E_2–E_1 splitting decreasing faster than the C_2–C_1: as expected, the dipolar approximation improves upon increasing the intermolecular distance.

Fig. 4 compares the energy of the four exciton states as obtained from ESM and TDDFT. Of course, the absolute energy needs a renormalization, but the r-dependence of the energies and the size of the splitting match fairly well. In spite of its

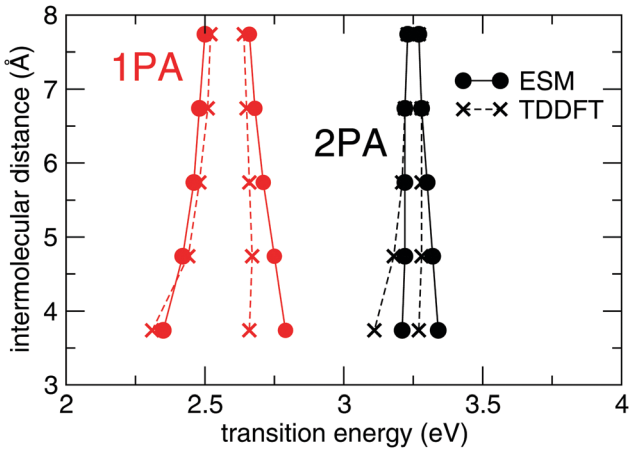

Fig. 4 1PA (red) and 2PA (black) transition energies calculated for the P–P curcumin dimer at variable intermolecular distances. ESM results (circles) are compared with TDDFT results (crosses). To facilitate the comparison, TDDFT results are rigidly downshifted by 0.83 eV for 2PA and by 0.69 eV for 1PA.

Table 4 ESM results on curcumin **1** and its dimer. Essential-state parameters for **1**: η = 0.94 eV; τ = 0.93 eV, μ_0 = 20 D, Γ = 0.28 eV

Monomer			
	Trans. en. [eV]	Osc. strength	δ_{2PA} [a.u.] (σ_{2PA} [GM])
C	2.56	0.8	0
E	3.23	0	4.4×10^5 (1100)

	Dimer r = 3.74 Å			Dimer r = 6.74 Å		
	Trans. en. [eV]	Osc. strength	δ_{2PA} [a.u.] (σ_{2PA} [GM])	Trans. en. [eV]	Osc. strength	δ_{2PA} [a.u.] (σ_{2PA} [GM])
C_1	2.35	0	0	2.48	0	0
C_2	2.79	1.6	0	2.68	1.6	0
E_1	3.21	0	0	3.22	0	0
E_2	3.34	0	2.9×10^5 (830)	3.28	0	4.8×10^5 (1360)

simplicity, ESM offers a reliable description of spectroscopic effects of intermolecular interactions for both allowed and dark states, suggesting that, whereas CT states enter into play at close distances, their effect on spectral properties can be neglected to a first approximation. Similar results are obtained for the T–P (non-equivalent monomers) dimer, as discussed in the ESI.†

Having validated ESMs on dimers, we now attack bigger aggregates, well beyond TDDFT capabilities, as needed for comparing with experimental data. We consider one-dimensional arrays of equivalent molecules (Fig. 5, left panels), accounting for nearest-neighbor interactions. While this represents an oversimplified view of the system, most of experimental results can be rationalized on this basis. To mimic the experimental geometry, we fix the intermolecular distance to 4 Å and a lateral shift of 3 Å. The results displayed in the top panels of Fig. 5 show a marked hypsochromic effect, as expected for H-aggregates, with the bright 1PA state blue-shifted with respect to the monomer. Moreover, the presence of a dark state at low energy (the position of the dark state is marked by a star in Fig. 5a) supports suppressed fluorescence in the aggregate. For comparison, the lower panels of Fig. 5 show the results for a different geometry, where the relative lateral shift of the molecules amounts to 13 Å. In this case, corresponding to a J-aggregate, the bright 1PA state is red-shifted with respect to the monomer, and, being the lowest excited state, supports good fluorescence properties of the aggregate.

ESM results displayed in Fig. 5a are obtained for a geometry that mimics the experimental crystallographic geometry (most probably similar to the geometry in the ONPs) and, predicting H-type behavior, agree well with experimental data. Indeed experimental absorption spectra of organic nanoparticles are blue-shifted with respect to the solvated dye, and the fluorescence of both powders and nanoparticles is largely suppressed (the residual red-shifted fluorescence observed in powders and nanoparticles can be ascribed to the activation of the dark state in Fig. 5a, due to molecular vibrations or minor deviations from the perfect alignment). Experimental 2PA of nanoparticles is marginally affected by intermolecular interactions. In agreement with the experiment, ESM results predict minor spectral shifts on 2PA bands.

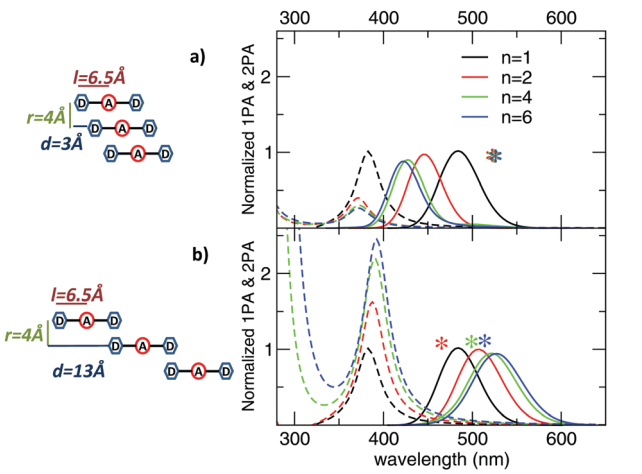

Fig. 5 Left panels: sketch of geometrical arrangements of aggregates of curcumins and geometrical parameters. Right panels: calculated spectra for selected geometries of curcumin dimers. *n* is the number of molecules. Continuous and dashed lines refer to 1PA and 2PA spectra, respectively. The * marks the position of the lowest energy dark state (C_1). In order to compare the results obtained for systems of different dimensions, 1PA and 2PA intensities were divided by the number of molecules.

Squaraines: systems with high quadrupolar character

Squaraines are popular systems for nonlinear optical applications, particularly for their large 2PA cross-section.[38–45] Squaraines, characterized by a large mixing of the N and Z_+ states and a marginal solvatochromism in absorption and emission belong to class II quadrupolar dyes. Their 1PA-active state, lying approximately at half the energy of the 2PA-active state, is responsible for a large (pre)resonance amplification of the 2PA band.[19,42] The large mixing of the diabatic basis states makes squaraines strongly polarizable, so that important deviations from the exciton model are expected. As discussed in the literature, TDDFT does not provide reliable results for squaraines mainly due to the biradicaloid character of the dye.[67–69] Therefore, we will not present TDDFT results for squaraine aggregates but will rely on ESMs. The resulting description of squaraines is somewhat oversimplified, but ESMs do not suffer from the drawback of TDDFT with biradicaloid and, while they do not account for localized excitations (including the excitations that involve the oxyallyl ring[67]), they capture the basic physics of the low-energy transitions of squaraine dyes,[19,80,81] offering a simple strategy to account for the subtle role of the molecular polarizability in aggregates.

We start our analysis with a rationalization of old results on squaraine dimers in controlled geometry.[66] Three different geometries are explored: a rigid dimer where a face-to-face arrangement is forced by a double bridge (CSq_mX); a series of dimers linked by a polymethylene spacer of increasing length (SqM_nSq, n = 2–10) and a series of xylyl-bridged dimers (SqX_xSq, x = *o*-, *m*-, *p*-). CSq_mX shows a blue-shifted band with respect to the monomer and is non-fluorescent, as expected for H-aggregates. In the SqM_nSq series, two absorption bands are observed, a blue-shifted band with respect to the monomer and a more intense red-shifted band (for n = 10, a single band is observed, at the same energy as the monomer, suggesting negligible interchromophore interactions). A red-shifted fluorescence is observed compared to the monomer, whose intensity is strongly suppressed for short spacers. A similar behavior is also observed for SqX_xSq.

The observation of intense red-shifted absorption and suppressed fluorescence, observed for both SqM_nSq and SqX_xSq series, is hard to rationalize in the exciton picture that, for aggregates showing a red-shifted absorption, also predicts good fluorescence properties (J-aggregates). This strange result can be rationalized by ESMs, as shown by results displayed in Fig. 6 (see also Fig. S16 in the ESI†). In ESMs, the isolated chromophore is parameterized against experimental data, setting η = 0.44 eV and τ = 1.05 eV.[81] In the faced geometry (Fig. 6a) as relevant to CSq_mX, the 1PA-active state of the monomers splits into a

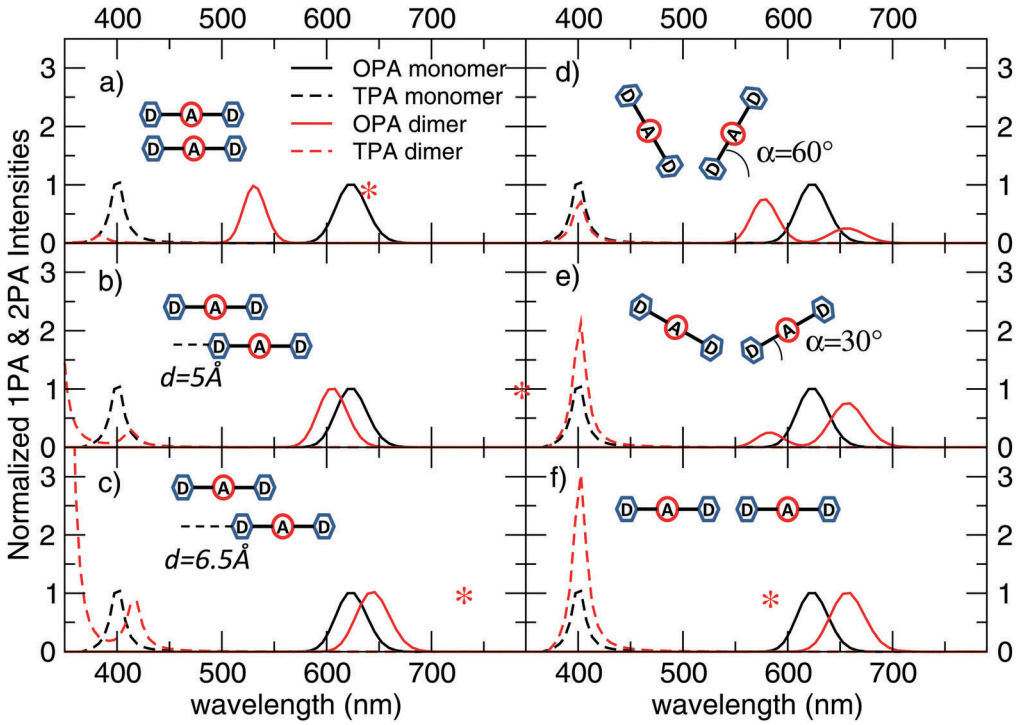

Fig. 6 Calculated spectra for selected geometries (panels a–f) of dimers of squaraine **2**. The * indicates the spectral position of the lowest dark state c (* is not shown in panels (d) and (e), since both c-states are bright). ESM parameters: η = 0.44 eV and τ = 1.05 eV. The length of the molecular arm is fixed to 5 Å. In left panels the distance between the two molecular axes is 5 Å. In right panels, the distance between the closest D groups is 5 Å.

bright state to the blue and a dark state to the red, explaining the fully suppressed fluorescence for the dimer CSq_mX in ref. 66. To describe SqM_nSq we can assume a "fan" geometry (Fig. 6d and e): in this case, both exciton states that originated from the c-state of the monomer are 1PA-active with relative intensities depending on the folding angle: for $\alpha < 45^\circ$, the red-shifted state dominates the 1PA spectrum, while for $\alpha > 45^\circ$, the blue-shifted state gives rise to a more intense transition, suggesting a suppression of fluorescence. Neither of the two cases is fully consistent with experiment. For a ladder-geometry (Fig. 6c), ESM predicts instead an intense red-shifted absorption band and at the same time a suppression of fluorescence due to the presence of a dark state further to the red. In this case, however, the model does not predict any blue-shifted absorption band. To rationalize the experimental data we suggest that in solution geometries as in Fig. 6c and e coexist.

Xylyl-bridged dimers, SqX_xSq, show two 1PA bands for the red and the blue of the monomer absorption and a similar fluorescence quantum yield as the monomer. The highest fluorescence quantum yield is observed in SqX_pSq, where the two chromophores are in the *para* position, and it decreases by a factor of 1.5 and 2.5 in SqX_mSq (*meta*) and SqX_oSq (*ortho*). Based on the available experimental data, SqX_pSq, SqX_mSq and SqX_oSq can be described by the geometrical arrangement in Fig. 6f, e and d respectively. For SqX_pSq, the second absorption band is dark in calculation, but it can acquire some intensity introducing molecular vibrations or interactions with the solvent.

In a recent paper, Belfield and coworkers investigate squaraine aggregates in water, observing a blue-shifted absorption and a strong decrease of fluorescence intensity, supporting the formation of H-aggregates.[40] The addition of a polyelectrolyte to the solution of the (cationic) squaraine leads to a strong red-shifted absorption and a complete suppression of fluorescence, a phenomenon ascribed to the formation of a "non-fluorescent J-aggregate".[40] The 2PA signal of the monomer and the H-aggregate is negligible in the 400–500 nm region, while an intense 2PA absorption (~460 GM) is observed in the presence of the polyelectrolyte (unfortunately the full shape of the 2PA band is not experimentally accessible due to resonance effects). The two observations of suppressed fluorescence in J-aggregates and the sizable effects on 2PA both contrast sharply with the exciton picture, but are naturally rationalized within ESM. For the squaraines investigated in ref. 40 (molecule **3** in Fig. 1) we set up the molecular model fixing η = 0.164 eV and τ = 1.2 eV. Fig. 7 shows 1PA and 2PA spectra calculated for a ladder geometry with a large lateral shift (6.5 Å). Similarly to results shown in Fig. 6c, where both dimer states that steam from the 1PA-active monomer states are red-shifted with respect to the monomer and the lowest-energy state is a dark state. For the ladder geometry, we then expect a strong suppression of the fluorescence (as for an H-aggregate) even if the observed absorption is red-shifted (as for a J-aggregate). The reason for this anomalous behavior is in the large polarizability of squaraines: because of the electrostatic interaction with the surrounding molecules, a squaraine molecule readjusts its charge distribution, leading to a variation of the transition frequency of each chromophore in the aggregate. For the aggregate in Fig. 7 we calculate the absorption spectrum in the mean-field approximation for a molecule experiencing the

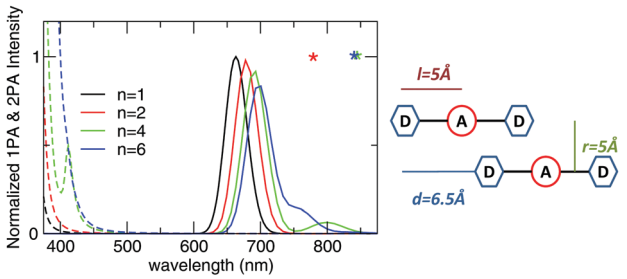

Fig. 7 Left panel: ESM calculation for aggregates of molecule **3** (parameters: η = 0.064 eV and τ = 1.2 eV); n is the number of molecules. Continuous and dashed lines refer to one-photon and two-photon absorption spectra, respectively. The * refers to the lowest (in energy) dark state. The molecule was parameterized in the framework of ESM in ref. 81. Here we have renormalized the parameters to have the same quadrupolar character without accounting for molecular vibrations in a nonpolar solvent. Right panel: sketch of geometrical arrangements of aggregates and geometrical parameters.

electric field generated by the surrounding molecules (see Fig. S17, ESI†) and obtain a very large red-shift of the absorption band with respect to the gas-phase monomer. The exciton splitting with respect to the mean-field absorption would then lead to a blue-shifted intense absorption and a red-shifted dark state, as in a classical H-aggregate, even if both transitions are red-shifted, when compared to the isolated dye. ESMs then provide a simple interpretation for the puzzling experimental observation of non-fluorescent J-aggregates in ref. 40: the red-shifted absorption band in the aggregate is not due to the lowest energy state in the exciton band (as found in traditional fluorescent J-aggregates), it is rather due to the highest energy state in the exciton band (as in traditional non-fluorescent H-aggregates). The observed red-shift is ascribed under these conditions to an overall red-shift of the whole exciton band with respect to the isolated molecule due to mean field effects, which are very strong in aggregates of largely polarizable dyes like squaraines. In this context, the definition of J- and H-aggregates becomes hardly applicable when referred to highly polarizable molecules, as already pointed out in ref. 25 Our results also agree with experimental 2PA data: indeed, according to Fig. 7, the 2PA cross-section is negligible in the 400–500 nm spectral region for the monomer and the dimer, but it increases for big aggregates.

Conclusions

The extensive analysis of experimental results on several families of aggregates of quadrupolar dyes, also supported by TDDFT results on dimeric structures, gives confidence about the possibility to reliably model and rationalize the properties of molecular aggregates fully accounting for the molecular polarizability and relaxing the dipolar approximation. ESMs fairly naturally lend themselves to this aim, offering a versatile alternative to the exciton model to deal with large molecular aggregates.

Quadrupolar dyes are of special interest for 2PA applications, and controlling the aggregation phenomena in quadrupolar-based aggregates and/or ONPs has a potential big impact on two-photon microscopy applications. In this respect, it is of paramount importance to understand the aggregation effects on both 2PA spectra and on the fluorescence quantum yield: the two-photon brilliance as relevant to microscopy applications is in fact defined as the product of the 2PA intensity times the fluorescence quantum yield. According to our results, for one-dimensional structures, the 2PA intensity can be amplified considerably if quadrupolar dyes are set in an aligned geometry or, at least, in a face-to-face geometry with a large lateral shift (ladder geometry). Quite interestingly, the aligned geometry shall also lead to brightly fluorescent aggregates, while in the ladder geometry we expect a suppressed fluorescence. An amplification of the 2PA response while maintaining good fluorescence properties can be obtained in a two-dimensional brickwork arrangement, as reported in ref. 90. In this paper, the authors demonstrate the formation of strongly fluorescent J-aggregates of quadrupolar dyes and the concomitant amplification of the 2PA cross-section. Preliminary results on 2D structures are reported in the ESI† (Fig. S18): the results are promising and are in agreement with experimental data. The investigation of brickwork structures deserves more attention, in order to thoroughly understand the relationship between structure and properties, and will be the subject of future work.

The recurrent observation of non-fluorescent J-aggregates of squaraines or, to be more precise, aggregates where, in spite of a red-shifted absorption, the fluorescence is strongly suppressed, calls for explanations well beyond the exciton model. Recently, this behavior has been ascribed to the effect of important intermolecular CT interactions,[25] and for sure this is a possibility in some systems. However, even in the absence of intermolecular CT interactions, ESMs support non-fluorescent J-aggregates due to the large polarizability of squaraine molecules. In aggregates of highly polarizable molecules, not only the exciton model is hardly applicable, but the very same definition of J- and H-aggregates is misleading.

Acknowledgements

The research leading to these results received funding from the People Programme (Marie Curie Actions) of the European Union's Seventh Framework Programme FP7/2007–2013 under REA grant agreement no. 607721 (Nano2Fun). This work was partially supported by Italian MIUR through PRIN2012T9XHH7_002 and by CINECA through IsC35_MMMOptic.

Notes and references

1 *Principles of Fluorescence Spectroscopy*, ed. J. R. Lakowicz, Springer US, Boston, MA, 2006.
2 B. Valeur, *Molecular Fluorescence*, Wiley-VCH Verlag GmbH, Weinheim, FRG, 2001.
3 T. Renger, *Photosynth. Res.*, 2009, **102**, 471–485.
4 A. S. Davydov, *Theory of Molecular Excitons*, Plenum Press, New York, 1971.

5 V. M. Agranovich and M. D. Galanin, *Electronic Excitation Energy Transfer in Condensed Matter*, North-Holland, Amsterdam, 1982, vol. 3909, p. 371.
6 T. Förster, *Ann. Phys.*, 1948, **437**, 55–75.
7 T. Förster, *Modern quantum chemistry*, Academic Press, 1965, p. 93.
8 K. Mukai, S. Abe and H. Sumi, *J. Phys. Chem. B*, 1999, **103**, 6096–6102.
9 K. F. Wong, B. Bagchi and P. J. Rossky, *J. Phys. Chem. A*, 2004, **108**, 5752–5763.
10 T. I. Hukka, T. Toivonen, E. Hennebicq, J.-L. Brédas, R. A. J. Janssen and D. Beljonne, *Adv. Mater.*, 2006, **18**, 1301–1306.
11 D. Beljonne, C. Curutchet, G. D. Scholes and R. J. Silbey, *J. Phys. Chem. B*, 2009, **113**, 6583–6599.
12 C. Sissa, A. K. Manna, F. Terenziani, A. Painelli and S. K. Pati, *Phys. Chem. Chem. Phys.*, 2011, **13**, 12734–12744.
13 F. Terenziani, G. D'Avino and A. Painelli, *ChemPhysChem*, 2007, **8**, 2433–2444.
14 G. D'Avino, F. Terenziani and A. Painelli, *J. Phys. Chem. B*, 2006, **110**, 25590–25592.
15 A. Painelli and F. Terenziani, *J. Am. Chem. Soc.*, 2003, **125**, 5624–5625.
16 F. Terenziani and A. Painelli, *Phys. Rev. B: Condens. Matter Mater. Phys.*, 2003, **68**, 165405.
17 A. Painelli, *Chem. Phys. Lett.*, 1998, **285**, 352–358.
18 A. Painelli and F. Terenziani, *Chem. Phys. Lett.*, 1999, **312**, 211–220.
19 F. Terenziani, A. Painelli, C. Katan, M. Charlot and M. Blanchard-Desce, *J. Am. Chem. Soc.*, 2006, **128**, 15742–15755.
20 F. Terenziani, C. Sissa and A. Painelli, *J. Phys. Chem. B*, 2008, **112**, 5079–5087.
21 L. Grisanti, C. Sissa, F. Terenziani, A. Painelli, D. Roberto, F. Tessore, R. Ugo, S. Quici, I. Fortunati, E. Garbin, C. Ferrante and R. Bozio, *Phys. Chem. Chem. Phys.*, 2009, **11**, 9450–9457.
22 J. Campo, A. Painelli, F. Terenziani, T. Van Regemorter, D. Beljonne, E. Goovaerts and W. Wenseleers, *J. Am. Chem. Soc.*, 2010, **132**, 16467–16478.
23 S. A. Kurhuzenkau, A. W. Woodward, S. Yao, K. D. Belfield, Y. O. Shaydyuk, C. Sissa, M. V. Bondar and A. Painelli, *Phys. Chem. Chem. Phys.*, 2016, **18**, 12839–12846.
24 C. Sissa, V. Calabrese, M. Cavazzini, L. Grisanti, F. Terenziani, S. Quici and A. Painelli, *Chem. – Eur. J.*, 2013, **19**, 924–935.
25 N. J. Hestand, C. Zheng, A. R. Penmetcha, B. Cona, J. A. Cody, F. C. Spano and C. J. Collison, *J. Phys. Chem. C*, 2015, **119**, 18964–18974.
26 C. Sissa, F. Terenziani, A. Painelli, A. K. Manna and S. K. Pati, *Chem. Phys.*, 2012, **404**, 9–15.
27 C. Sissa, F. Terenziani, A. Painelli, A. Abbotto, L. Bellotto, C. Marinzi, E. Garbin, C. Ferrante and R. Bozio, *J. Phys. Chem. B*, 2010, **114**, 882–893.
28 F. Todescato, I. Fortunati, S. Carlotto, C. Ferrante, L. Grisanti, C. Sissa, A. Painelli, A. Colombo, C. Dragonetti and D. Roberto, *Phys. Chem. Chem. Phys.*, 2011, **13**, 11099–11109.
29 A. Painelli, F. Terenziani, L. Angiolini, T. Benelli and L. Giorgini, *Chem. – Eur. J.*, 2005, **11**, 6053–6063.
30 F. Terenziani, M. Morone, S. Gmouh and M. Blanchard-Desce, *ChemPhysChem*, 2006, **7**, 685–696.
31 F. Terenziani, O. Mongin, C. Katan, B. K. G. Bhatthula and M. Blanchard-Desce, *Chem. – Eur. J.*, 2006, **12**, 3089–3102.
32 F. Terenziani, S. Ghosh, A.-C. Robin, P. K. Das and M. Blanchard-Desce, *J. Phys. Chem. B*, 2008, **112**, 11498–11505.
33 F. Terenziani, V. Parthasarathy, A. Pla-Quintana, T. Maishal, A. M. Caminade, J. P. Majoral and M. Blanchara-Desce, *Angew. Chem., Int. Ed.*, 2009, **48**, 8691–8694.
34 V. Parthasarathy, R. Pandey, F. Terenziani, P. K. Das and M. Blanchard-Desce, *Phys. Chem. Chem. Phys.*, 2014, **16**, 9096.
35 G. D'Avino, L. Grisanti, J. Guasch, I. Ratera, J. Veciana and A. Painelli, *J. Am. Chem. Soc.*, 2008, **130**, 12064–12072.
36 G. D'Avino, L. Grisanti, A. Painelli, J. Guasch, I. Ratera and J. Veciana, *CrystEngComm*, 2009, **11**, 2040.
37 J. Guasch, L. Grisanti, S. Jung, D. Morales, G. D'Avino, M. Souto, X. Fontrodona, A. Painelli, F. Renz, I. Ratera and J. Veciana, *Chem. Mater.*, 2013, **25**, 808–814.
38 S. Sreejith, P. Carol, P. Chithra and A. Ajayaghosh, *J. Mater. Chem.*, 2008, **18**, 264–274.
39 L. Beverina and P. Salice, *Eur. J. Org. Chem.*, 2010, 1207.
40 Y. Zhang, B. Kim, S. Yao, M. V. Bondar and K. D. Belfield, *Langmuir*, 2013, **29**, 11005–11012.
41 H.-Y. Ahn, S. Yao, X. Wang and K. D. Belfield, *ACS Appl. Mater. Interfaces*, 2012, **4**, 2847–2854.
42 J. Fu, L. A. Padilha, D. J. Hagan, E. W. Van Stryland, O. V. Przhonska, M. V. Bondar, Y. L. Slominsky and A. D. Kachkovski, *J. Opt. Soc. Am. B*, 2007, **24**, 67.
43 S. Webster, J. Fu, L. A. Padilha, O. V. Przhonska, D. J. Hagan, E. W. Van Stryland, M. V. Bondar, Y. L. Slominsky and A. D. Kachkovski, *Chem. Phys.*, 2008, **348**, 143–151.
44 D. Scherer, R. Dörfler, A. Feldner, T. Vogtmann, M. Schwoerer, U. Lawrentz, W. Grahn and C. Lambert, *Chem. Phys.*, 2002, **279**, 179–207.
45 S. Ohira, I. Rudra, K. Schmidt, S. Barlow, S.-J. Chung, Q. Zhang, J. Matichak, S. R. Marder and J.-L. Brédas, *Chem. – Eur. J.*, 2008, **14**, 11082–11091.
46 J. Daniel, A. G. Godin, M. Palayret, B. Lounis, L. Cognet and M. Blanchard-Desce, *J. Phys. D: Appl. Phys.*, 2016, **49**, 084002.
47 J. M. Hales, D. J. Hagan, E. W. Van Stryland, K. J. Schafer, A. R. Morales, K. D. Belfield, P. Pacher, O. Kwon, E. Zojer and J. L. Bredas, *J. Chem. Phys.*, 2004, **121**, 3152–3160.
48 C. D. Andrade, C. O. Yanez, L. Rodriguez and K. D. Belfield, *J. Org. Chem.*, 2010, **75**, 3975–3982.
49 C. Rouxel, M. Charlot, Y. Mir, C. Frochot, O. Mongin and M. Blanchard-Desce, *New J. Chem.*, 2011, **35**, 1771.
50 O. Mongin, L. Porrès, M. Charlot, C. Katan and M. Blanchard-Desce, *Chem. – Eur. J.*, 2007, **13**, 1481–1498.
51 M. Charlot, N. Izard, O. Mongin, D. Riehl and M. Blanchard-Desce, *Chem. Phys. Lett.*, 2006, **417**, 297–302.
52 H. Y. Woo, B. Liu, B. Kohler, D. Korystov, A. Mikhailovsky and G. C. Bazan, *J. Am. Chem. Soc.*, 2005, **127**, 14721–14729.
53 S. J. K. Pond, M. Rumi, M. D. Levin, T. C. Parker, D. Beljonne, M. W. Day, J.-L. Brédas, S. R. Marder and J. W. Perry, *J. Phys. Chem. A*, 2002, **106**, 11470–11480.
54 B. Strehmel, A. M. Sarker and H. Detert, *ChemPhysChem*, 2003, **4**, 249–259.

55 Y. Tian, C.-Y. Chen, Y.-J. Cheng, A. C. Young, N. M. Tucker and A. K.-Y. Jen, *Adv. Funct. Mater.*, 2007, **17**, 1691–1697.
56 M. Montalti, L. Prodi, E. Rampazzo and N. Zaccheroni, *Chem. Soc. Rev.*, 2014, **43**, 4243.
57 T. O. McDonald, P. Martin, J. P. Patterson, D. Smith, M. Giardiello, M. Marcello, V. See, R. K. O'Reilly, A. Owen and S. Rannard, *Adv. Funct. Mater.*, 2012, **22**, 2469–2478.
58 V. Parthasarathy, S. Fery-Forgues, E. Campioli, G. Recher, F. Terenziani and M. Blanchard-Desce, *Small*, 2011, **7**, 3219–3229.
59 E. Campioli, C. Rouxel, M. Campanini, L. Nasi, M. Blanchard-Desce and F. Terenziani, *Small*, 2013, **9**, 1982–1988.
60 E. Campioli, D. M. Nikolaidou, V. Hugues, M. Campanini, L. Nasi, M. Blanchard-Desce and F. Terenziani, *J. Mater. Chem. C*, 2015, **3**, 7483–7491.
61 D. Horn and J. Rieger, *Angew. Chem., Int. Ed.*, 2001, **40**, 4330.
62 J. Zhang, R. Chen, Z. Zhu, C. Adachi, X. Zhang and C.-S. Lee, *ACS Appl. Mater. Interfaces*, 2015, **7**, 26266–26274.
63 A. D'Aléo, A. Felouat, V. Heresanu, A. Ranguis, D. Chaudanson, A. Karapetyan, M. Giorgi and F. Fages, *J. Mater. Chem. C*, 2014, **2**, 5208–5215.
64 L. Aparicio-Ixta, M. Rodriguez and G. Ramos-Ortiz, *Contemporary Optoelectronics*, 2016, pp. 25–50.
65 J. Rodríguez-Romero, L. Aparicio-Ixta, M. Rodríguez, G. Ramos-Ortíz, J. L. Maldonado, A. Jiménez-Sánchez, N. Farfán and R. Santillan, *Dyes Pigm.*, 2013, **98**, 31–41.
66 K. Liang, M. S. Farahat, J. Perlstein, K.-Y. Law and D. G. Whitten, *J. Am. Chem. Soc.*, 1997, **119**, 830–831.
67 K. Srinivas, C. Prabhakar, C. Lavanya Devi, K. Yesudas, K. Bhanuprakash and V. Jayathirtha Rao, *J. Phys. Chem. A*, 2007, **111**, 3378–3386.
68 G. Krishna Chaitanya, A. L. Puyad and K. Bhanuprakash, *RSC Adv.*, 2015, **5**, 18813–18821.
69 J. Fabian, *Dyes Pigm.*, 2010, **84**, 36–53.
70 M. J. Frisch, G. W. Trucks, H. B. Schlegel, G. E. Scuseria, M. A. Robb, J. R. Cheeseman, G. Scalmani, V. Barone, B. Mennucci, G. A. Petersson, H. Nakatsuji, M. Caricato, X. Li, H. P. Hratchian, A. F. Izmaylov, J. Bloino, G. Zheng, J. L. Sonnenberg, M. Hada, M. Ehara, K. Toyota, R. Fukuda, J. Hasegawa, M. Ishida, T. Nakajima, Y. Honda, O. Kitao, H. Nakai, T. Vreven, J. A. Montgomery Jr., J. E. Peralta, F. Ogliaro, M. Bearpark, J. J. Heyd, E. Brothers, K. N. Kudin, V. N. Staroverov, R. Kobayashi, J. Normand, K. Raghavachari, A. Rendell, J. C. Burant, S. S. Iyengar, J. Tomasi, M. Cossi, N. Rega, J. M. Millam, M. Klene, J. E. Knox, J. B. Cross, V. Bakken, C. Adamo, J. Jaramillo, R. Gomperts, R. E. Stratmann, O. Yazyev, A. J. Austin, R. Cammi, C. Pomelli, J. W. Ochterski, R. L. Martin, K. Morokuma, V. G. Zakrzewski, G. A. Voth, P. Salvador, J. J. Dannenberg, S. Dapprich, A. D. Daniels, Ö. Farkas, J. B. Foresman, J. V. Ortiz, J. Cioslowski and D. J. Fox, Gaussian Inc., Wallingford CT, 2009.
71 A. D. Becke, *Phys. Rev. A: At., Mol., Opt. Phys.*, 1988, **38**, 3098–3100.
72 J.-D. Chai and M. Head-Gordon, *Phys. Chem. Chem. Phys.*, 2008, **10**, 6615.
73 J. Tomasi, B. Mennucci and R. Cammi, *Chem. Rev.*, 2005, **105**, 2999–3094.
74 T. Yanai, D. P. Tew and N. C. Handy, *Chem. Phys. Lett.*, 2004, **393**, 51–57.
75 K. Aidas, C. Angeli, K. L. Bak, V. Bakken, R. Bast, L. Boman, O. Christiansen, R. Cimiraglia, S. Coriani, P. Dahle, E. K. Dalskov, U. Ekström, T. Enevoldsen, J. J. Eriksen, P. Ettenhuber, B. Fernández, L. Ferrighi, H. Fliegl, L. Frediani, K. Hald, A. Halkier, C. Hättig, H. Heiberg, T. Helgaker, A. C. Hennum, H. Hettema, E. Hjertenaes, S. Høst, I.-M. Høyvik, M. F. Iozzi, B. Jansík, H. J. A. Jensen, D. Jonsson, P. Jørgensen, J. Kauczor, S. Kirpekar, T. Kjaergaard, W. Klopper, S. Knecht, R. Kobayashi, H. Koch, J. Kongsted, A. Krapp, K. Kristensen, A. Ligabue, O. B. Lutnaes, J. I. Melo, K. V. Mikkelsen, R. H. Myhre, C. Neiss, C. B. Nielsen, P. Norman, J. Olsen, J. M. H. Olsen, A. Osted, M. J. Packer, F. Pawlowski, T. B. Pedersen, P. F. Provasi, S. Reine, Z. Rinkevicius, T. A. Ruden, K. Ruud, V. V. Rybkin, P. Sałek, C. C. M. Samson, A. S. de Merás, T. Saue, S. P. A. Sauer, B. Schimmelpfennig, K. Sneskov, A. H. Steindal, K. O. Sylvester-Hvid, P. R. Taylor, A. M. Teale, E. I. Tellgren, D. P. Tew, A. J. Thorvaldsen, L. Thøgersen, O. Vahtras, M. A. Watson, D. J. D. Wilson, M. Ziolkowski and H. Ågren, *Wiley Interdiscip. Rev.: Comput. Mol. Sci.*, 2014, **4**, 269–284.
76 P. R. Monson, *J. Chem. Phys.*, 1970, **53**, 29.
77 C.-K. Wang, K. Zhao, Y. Su, Y. Ren, X. Zhao and Y. Luo, *J. Chem. Phys.*, 2003, **119**, 1208.
78 M. Sun, J. Chen and H. Xu, *J. Chem. Phys.*, 2008, **128**, 064106.
79 F. Terenziani, O. V. Przhonska, S. Webster, L. A. Padilha, Y. L. Slominsky, I. G. Davydenko, A. O. Gerasov, Y. P. Kovtun, M. P. Shandura, A. D. Kachkovski, D. J. Hagan, E. W. Van Stryland and A. Painelli, *J. Phys. Chem. Lett.*, 2010, **1**, 1800–1804.
80 C. Sissa, F. Terenziani, A. Painelli, R. B. K. Siram and S. Patil, *J. Phys. Chem. B*, 2012, **116**, 4959–4966.
81 K. M. Shafeekh, S. Das, C. Sissa and A. Painelli, *J. Phys. Chem. B*, 2013, **117**, 8536–8546.
82 H. Hu, O. V. Przhonska, F. Terenziani, A. Painelli, D. Fishman, T. R. Ensley, M. Reichert, S. Webster, J. L. Bricks, A. D. Kachkovski, D. J. Hagan and E. W. Van Stryland, *Phys. Chem. Chem. Phys.*, 2013, **15**, 7666.
83 C. Sissa, P. M. Jahani, Z. G. Soos and A. Painelli, *ChemPhysChem*, 2012, **13**, 2795–2800.
84 B. J. Orr and J. F. Ward, *Mol. Phys.*, 1971, **20**, 513–526.
85 C. Sissa, V. Parthasarathy, D. Drouin-Kucma, M. H. V Werts, M. Blanchard-Desce and F. Terenziani, *Phys. Chem. Chem. Phys.*, 2010, **12**, 11715–11727.
86 A. Felouat, A. D'Aléo and F. Fages, *J. Org. Chem.*, 2013, **78**, 4446–4455.
87 K. Kamada, T. Namikawa, S. Senatore, C. Matthews, P.-F. Lenne, O. Maury, C. Andraud, M. Ponce-Vargas, B. Le Guennic, D. Jacquemin, P. Agbo, D. D. An, S. S. Gauny, X. Liu, R. J. Abergel, F. Fages and A. D'Aléo, *Chem. – Eur. J.*, 2016, **22**, 5219–5232.
88 G. Ponterini, D. Vanossi, Z. A. Krasnaya, A. S. Tatikolov and F. Momicchioli, *Phys. Chem. Chem. Phys.*, 2011, **13**, 9507.
89 F. Santoro, R. Improta, A. Lami, J. Bloino and V. Barone, *J. Chem. Phys.*, 2007, **126**, 084509.
90 Z. Xu, Q. Liao, Y. Wu, W. Ren, W. Li, L. Liu, S. Wang, Z. Gu, H. Zhang and H. Fu, *J. Mater. Chem.*, 2012, **22**, 17737.

